tubular columns under horizontal impact

Jun Wang; Zhilin Chen; Hota GangaRao; Ruifeng Liang; Weiqing Liu **Abstract**: This paper presents the experimental and analytical results of concrete-filled fiber-reinforced polymer (FRP) tubes (CFFTs) and concrete filled GFRP-steel double skin tubular columns (DSTCs) under horizontal impact loads. The influences of the thickness of FRP tubes and impact velocity were discussed, and the impact responses of CFFTs were compared with those of concrete-filled FRP-steel DSTCs. The concrete-filled FRP-steel DSTCs exhibited more severe damage on the impact point and slighter damage at the fixed end, compared with CFFTs under the identical impact velocity. The thickness of the FRP tubes had insignificant influence on the peak impact load and the maximum displacement. Under the same applied impact energy, the maximum displacement of concrete filled FRP-steel DSTC specimens was ~40% smaller than that of CFFT specimens. The impact velocity has more significant influence on the peak impact load than the duration. Higher impact velocity caused heavier damage, thus resulting in larger unrecoverable deflections. A three-dimensional finite-element (FE) model was developed to simulate the impact behavior of two types of composite columns and the numerical results were compared with the test data. Then, the verified FE model was used to analyze the influence of axial compressive load and impact height. Based on Euler–Bernoulli beam theory, analytical solutions for lateral displacement of composite columns under impact were obtained, in which the impact loads were assumed as a dual function and the effect of impact damage was considered by introducing reduction factors into the vibration equations. The comparison of analytical results and test results showed that the maximum displacement could be accurately predicted by the proposed theoretical model.

Key Words: Horizontal impact; Glass fiber-reinforced polymer (GFRP) tubes; Concrete; Steel tubes; Analytical method; FE model

Introduction

Concrete filled fiber reinforced polymer (FRP) tubes (CFFTs) have been increasingly used as bridge piers, piles and fender systems due to their excellent behavior on load carrying capacity and ductility (Mirmiran and Shahawy 1996, Fam et al. 2003, GangaRao et al. 2007). The outer FRP tube not only provides the concrete core with a stay-in-place formwork during construction, but also provides hoop confinement which results in enhancement in concrete compressive strength. Moreover, FRP tubes help protect the concrete insulate from aqueous corrosion. Simultaneously, FRP-concrete steel double-skin tubular columns (DSTCs) proposed by Teng et al. (2017) are found to provide lighter self-weight, increase in section modulus, enhance stability and improve cyclic performance. DSTCs have wide range of application in structures such as bridges, high-rise buildings, viaducts and electricity transmission towers; hence the proposed approach becomes very important for designers of such structures. Both CFFTs and FRP-concrete steel DSTCs are susceptible to lateral impact from vehicles and vessels. However, few studies have been conducted to explore the impact behavior of hybrid composite columns. The literature is replete with studies on bearing capacity of concrete columns wrapped with FRP under axial compression (Lam and Teng 2003, Xie et al. 2011), bending (Dagher et al. 2012, Yu et al. 2006), and cycling loading (Li et al. 2013).

Recently, researchers have started to investigate the impact responses of hybrid composite columns, i.e., concrete-filled FRP tubes and FRP-steel tubes, as well as FRP-concrete steel DSTCs. Pham and Hao (2017) investigated the confinement mechanism of FRP confined columns under axial impacts. The rupture strain of glass fiber reinforced polymer (GFRP) is higher than that of carbon fiber reinforced polymer (CFRP), resulting in higher confinement efficiency of GFRP under impacts (Pham and Hao 2017). Qasrawi et al. (2015) investigated the dynamic behavior of CFFTs under lateral impact. Their test results indicated that the outer GFRP tube contributes to sharply increase the impact resistance and energy absorption, compared with the unconfined counterparts. Moreover, a single degree of freedom model was developed by Qasrawi et al. (2015) to predict the displacement histories CFFTs under impact, in which the damping and strain rate effects were considered. The studies of Huang et al. 2017, 2018 showed that with the increase of impact energy, the peak impact load of CFFTs with steel spiral reinforcement change unsignificantly, while the duration increased slightly.

For concrete-filled steel tubes (CFSTs) wrapped with FRP, Xiao and Shen 2012 studied the responses of CFSTs wrapped with CFRP under axial impact. The impact load versus time histories for CFSTs wrapped with CFRP are similar to those of CFSTs, and increasing the number of layers of CFRP results in enhancing the peak impact load and the duration of the impact (Xiao and Shen 2012). Alam et al. 2015 developed a finite element (FE) model to investigate the effect of bond length on the responses of CFRP strengthened CFTs under lateral impact. Their numerical results indicated that adhesive with high interfacial fracture energy contributes to minimize

the lateral displacement of the CFSTs wrapped with CFRP under impact. Moreover, the effective bonding length of a CFRP strengthened CFST column to resist impact load is influenced by the impact energy, CFRP properties, adhesive type and axial loading level (Alam et al. 2015). The impact tests of CFSTs wrapped with FRP conducted by Chen et al. 2015 confirmed that GFRP confined tubes absorbed more energy and had smaller deflection than the CFRP confined tubes

Limited studies have been conducted on the impact behavior of FRP-concrete steel DSTCs. Abdelkarim and ElGawady 2016 conducted a parametric study of FRP-concrete steel DSTC columns under vehicle collisions by LS-DYNA software. They stated that the peak impact load of FRP-concrete steel DSTC column was lower than that of the RC column by approximately 40% and 28% when it was impacted by a vehicle with a mass of 2 ton at a velocity of 70mph and 50 mph. Wang et al. 2015 carried out experimental study on FRP-concrete steel DSTC columns under lateral impact. Their test results indicated that the impact load history of FRP-concrete steel DSTCs is similar to that of concrete filled steel tubes and concrete filled double steel tubes (CFDSTs). Fracture of the FRP jackets and crushing of filled concrete dominated the failure of the FRP-concrete steel DSTCs under impact. However, shear failure of the outer steel tube dominated the failure of CFDSTs (Wang et al. 2015).

Drop weight impact testing is the most common test to evaluate impact data of composite structures, which most closely resembles impact damage in the field. It has the advantage of having inherent fail-safe characteristics when the test specimens are destroyed completely, as the vertical motion of the hammer can be impeded by anvil seated on the string floor (Aghdamy et al. 2016). The authors have conducted drop weight impact testing on hybrid composite columns, i.e. hollow and concrete filled GFRP tube columns (Wang et al. 2017), bare steel tubes, as well as hollow steel tubes wrapped with GFRP (Liu et al. 2018), to investigate their responses subjected to lateral impact. The peak impact loads of CFFTs were much higher than those of hollow GFRP tubes, whereas the hollow GFRP tunes exhibited almost the same energy absorption capacities as CFFTs under the same magnitude of impact energy (Wang et al. 2017). The prevalent damages in the hollow steel tubes are elephant's foot buckling at the clamped end and inwards at the loading point. However, shear failure of GFRP occurs at the clamped end of steel tubes wrapped with GFRP (Liu et al. 2018). In drop weight impact system, the dropping hammer impacts the specimens vertically, and shall separate with the specimens promptly. Otherwise, the impactor will move together with the test specimens. In this event, it is necessary to take into account the effects of the additional mass on the impact responses of specimens. Moreover, it requires increasing the applied impact energy by increasing the height of the free fall or the dropping weight which implies increasing the height of the tower or strengthening the vertical guiding columns (Aghdamy et al. 2016).

The objective of the present work is to investigate the behavior of CFFTs and FRP-concrete steel DSTCs by a horizontal trolley traction system (Fig.1). The effect

of wall thickness of outer FRP tubes coupled with impact velocity is discussed, and then the failure modes and impact responses of CFFTs are compared with those of FRP-concrete steel DSTCs. Based on the theory of vibration of continuous beams, analytical dynamic response models are developed in which the impact load is simulated by a linear function and an exponential function. The analytical results agree well with test results.

Experimental program

Materials

Filament-wound tubes were supplied by Hebei Chengda FRP Co., Ltd, China. The tubes were made of isophthalic polyester resin with unidirectional E-glass fibers at ±55° winding angle. The amount of resin volume percent was maintained close to 0.7. The tubes mechanical properties, obtained from the manufacturer, were a compressive strength of 161 MPa, a compressive modulus of 12 GPa, a Poisson's ration of 0.3, a tensile strength of 380 MPa, a tensile modulus of 35 GPa in the axial direction, and a tensile strength of 320 MPa, a tensile modulus of 31 GPa and a Poisson's ration of 0.22 in the hoop direction.

Cold-formed Q235 steel tubes were used in the construction of concrete filled GFRP-steel double skin tubular columns. Tensile tests were conducted following the GB/T 228.1-2010 to measure the material properties of the steel tubes. 0.2% proof stress of the steel was adopted as the yield stress. The test results showed that the steel tube has a yield stress of 278 MPa, Young's modulus of 201 GPa and Poisson's ratio of 0.3.

The filled concrete was from the same batch. Five cylinders with diameter of 150 mm and height of 300 mm were cast and cured under the conditions similar to the related columns. The compressive properties of the concrete were measured following ASTM C39/C39M – 12. The test results showed that the concrete has a compressive strength of 22.5 MPa, Young's modulus of 28 GPa and Poisson's ratio of 0.2.

Each specimen has a steel reinforced concrete abutment to fix the end of the column with the ground. HRB 400 steel rebars were used as reinforcement in concrete of the abutments. All the specimens and abutments were cast from the same batch of concrete, as shown in Fig.2 (a). The abutment was fixed with the concrete floor by four steel bolts with diameter of 45 mm and length of 800 mm. The fabricating process includes: 1) installing the timber formwork of the abutment; 2) assembling the steel rebars in the abutment; 3) fixing the GFRP tubes and steel tubes (only for DSTCs) with the steel rebars and 4) casting concrete in the columns and abutments. Fig.2 shows the fabrication process of the specimens.

Test specimen

Eight specimens were prepared to study structural response under impact loads, in which four specimens were concrete filled FRP tubular columns (CFFTs), and the others were concrete filled FRP-steel DSTCs. All the test specimens were of the same height (1560 mm) and GFRP inner diameter (300 mm). The thickness of GFRP tubes was taken as 7 mm and 10 mm, respectively, and the outer diameter and thickness of the steel tubes were taken as 140 mm and 3 mm, respectively. Table 1 shows the impact velocity and response data for all test specimens, including nomenclature abbreviations.

Experimental set-up

Impact systems consisted of a vertical drop weight and a horizontal trolley traction impact test machine were installed at the Advanced Engineering Composites Research Center at Nanjing Tech University, China. The details of the vertical drop weight system have been presented in Wang et al. (2017). The horizontal trolley traction system was used to test the impact behavior of CFFTs and concrete filled FRP-steel DSTCs. The horizontal impact system consists of reaction wall, guide rail and trolley traction device. The mass of the trolley is 1580 kg and the effective length of the rail is 23 m. When the trolley is accelerated to the designed velocity near the specimen, the cable is unhooked from the trolley, and then the trolley hit the specimen at a certain speed. The designed speed of trolley is related with the mass of drop hammer which can be varied from 200 kg to 1200 kg by the change of steel weights. The trolley has a maximum impact velocity of 8 m/s, and the applied impact energy can be varied from 1000 J to 230,000 J. In this paper, the authors tried three different impact velocities with small increment (i.e. 4 m/s, 5.5 m/s and 7 m/s) on three new specimens, respectively. After the impactor hit the specimen, the trolley was immediately separated from the test specimen. 61.9 kJ, 85.2 kJ, 108 kJ.

The time histories of the impact load were recorded by a piezoelectric sensor mounted between the impactor and the trolly. A Linear Variable Displacement Transducer (LVDT) was used to continuously record the lateral displacement data of loading position. An acceleration transducer was mounted on each specimen to check the force history. The test setup and measurement systems are shown in Fig. 3. In addition, a high speed video camera NEX-FS700RH produced by Sony Corporation was used to record the impact process at a speed of 400 frames per second.

Results and discussion

Damage mode

The impact damages of all the test specimens were located at the impact point and the fixed end, as shown in Fig.4. The damage at the loading point of CFFTs under the applied impact energy of 61.9 kJ (velocity=4 m/s) was insignificant, while the increase of applied impact energy resulted in extension of the damage at the loading point. Meanwhile, CFFTs under the applied impact energy of 61.9 kJ exhibited circular debondings between the concrete of abutment and GFRP tube. Typical failure

of the CFFTs under the applied impact energies of 85.2 kJ and 108 kJ was dominated by fiber rupture in the hoop direction at the fixed end of the GFRP tubes.

Under the same applied impact energy, the damage at the loading point of concrete filled FRP-steel DSTCs was more significant than that of CFFTs, which indicated that concrete filled FRP-steel DSTCs had smaller local stiffness than CFFTs. However, the damage area at the fixed end of the concrete filled FRP-steel DSTCs was smaller than that of CFFTs, due to the smaller stress in the fixed end of GFRP tube of concrete filled FRP-steel DSTCs.

Figs. 5 and 6 show the typical impact failure process (i.e.C7-II and D7-II) recorded by the high-speed video camera. C7-II experienced significant lateral deformation when it collided with the trolley. Then, with the increase of lateral deformation, the contact area between C7-II and the impactor was decreased, and the contact point of the column moved downwards, which resulted in the second impact. Heavy damage due to the impact resulted in high damping, thus causing permanent deformation in C7-II. However, the lateral deformation of D7-II was much smaller than that of C7-II. After the impactor was separated from the column, reciprocating vibration occurred in D7-II around the abutment.

Impact load history

The impact load-time history curves of CFFTs and concrete filled FRP-steel DSTCs were illustrated in Fig.7. At the very beginning of impact, the impact load of the CFFTs increased sharply to a peak value. Then, the impactor and the specimens moved forward together resulted in a plateau of the impact load. With the increase of global bending deformation of the specimens, the contact area between the impactor and specimen decreased and the contact point moved downward along the specimen, resulting in fluctuations of the impact load with time.

When the thickness of GFRP tubes increased from 7 to 10 mm, the peak impact load increased by 6% and 13% for CFFTs and concrete filled FRP-steel DSTCs, respectively, while the duration decreased by 28% and 11% for CFFTs and concrete filled FRP-steel DSTCs, respectively. It indicated that the thickness of GFRP tubes had insignificant effect on the peak impact load, especially for CFFTs. Such effect is attributed to the concrete core which carries most of impact load and GFRP tube has less effect compared with the concrete core. The specimen with thicker GFRP wall has higher local stiffness and damping leading to the decrease in duration. When the impact velocity increased from 4 m/s to 7 m/s, the peak impact loads of CFFTs and concrete filled FRP-steel DSTCs increased by 75%~84%, while the duration changed insignificantly.

In the case of the same applied impact energy, the P_{max} of concrete filled FRP-steel DSTC specimens was 8~15% higher than that of CFFT specimens, while the duration

of concrete filled FRP-steel DSTC specimens was around 30~50% shorter than that of CFFT specimens.

Displacement history

The displacement histories at impact loading location were measured, as shown in Fig.8. All specimens showed an increase in displacement as the load impacts the specimen, and then the displacement decreased and fluctuated at the residual deflection. The residual deformations of these two kinds of specimens were 35~70% of the maximum deformation, and higher applied impact energy caused heavier damage, thus resulting in higher residual deformations. The maximum displacement depended on the applied impact energy, duration and stiffness of the test specimens. Under the same applied impact energy, higher duration resulted in larger maximum displacement. However, the thickness of GFRP tubes has insignificant effect on the maximum displacement. Increasing the GFRP thickness from 7 mm to 10 mm merely led to the reduction of ~15% in maximum displacement of CFFT and concrete filled FRP-steel DSTC specimens. In addition, the maximum displacement of concrete filled FRP-steel DSTC specimens was ~40% smaller than that of CFFT specimens under the same applied impact energy.

Acceleration history

Figure 9 shows the acceleration and deceleration histories of the test specimens. Increasing the applied impact energy resulted in dramatic enhancement of the peak acceleration of CFFT and concrete filled FRP-steel DSTC specimens, while the thickness of the GFRP has insignificant influence on the peak acceleration. In the case of the same applied impact energy, the peak acceleration of concrete filled FRP-steel DSTC specimens was 15~76% larger than that of CFFTs. It indicated that the peak force of the specimens had a trend similar to the peak acceleration (Figs.7 and 9).

Impact energy

The energy absorption capacity can be obtained from the relationship of applied impact load and displacement,

$$U = \int P(w)dw \tag{1}$$

where P is applied impact load and w is displacement history at load point.

Table 1 lists energy absorption of test specimens. Increasing the impact velocity from 4 m/s to 5.5 and 7 m/s resulted in the enhancement of energy absorption of CFFT and concrete filled FRP-steel DSTC specimens by ~80% and ~150%, respectively. However, the thickness of GFRP tubes has insignificant influence on the energy absorption. Under the same impact velocity, the energy absorption of concrete filled FRP-steel DSTCs is 13%~20% higher than that of CFFTs.

Finite element simulation

In this section, a three dimension FE model has been developed using ANSYS/LS-DYNA to simulate the test results. Then, the verified FE model was used to analyze influences of impact locations and axial loads on the responses of CFFTs and concrete filled FRP-steel DSTCs.

Material models

Continuous surface cap model (MAT 159) was applied to describe the behavior of concrete core under impact, which includes several constitutive equations to consider the strain rate effect and hydrostatic pressure on the yield stress (Murrary 1993). This model is developed to simulate concrete-like materials used in fender systems at roadside when subjected collision loads induced by motor vehicles. It has been successfully used to capture the characteristic of reinforced concrete beams (Adhikary et al. 2015), ultra-high performance fiber reinforced beams (Guo et al. 2018) and concrete-encased concrete-filled steel tubes (Hu et al. 2018) under low-velocity impacts. When the unconfined compressive strength of concrete is in the range of 20~58 MPa and the aggregate sizes are from 8~32 mm, default parameters can be provided for concrete model based on the unconfined compressive strength of concrete, aggregate size and units (Adhikary et al. 2015). The input parameters for the concrete are listed in Table 2.

FRP material was simulated by "055-enhanced composite damage" model which presented a linear elastic behavior until failure. This model was selected for the present modeling study due to its relative simplicity as well as the superior performance in simulation of collision (Singh 2015). The Tsai-Wu criterion was selected to predict the failure of GFRP tubes.

The inner steel tubes were simulated by bilinear kinematic plasticity model (MAT_PLASTIC_KINEMATIC) with Von Mises yield criterion. The stress-strain curves of steel in elastic-plastic phase was simplified as a bi-linear relationship, contains formulations incorporating isotropic and kinetic hardening. The impactor was made of high strength steel, so it was modeled as a rigid object with a mass of 1580 kg, modulus of 210 GPa and a Possion's ratio of 0.3.

FE model construction

The concrete and impactor were modeled by Solid 164 3-D solid element, while GFRP and steel tubes were modeled by Shell 163 element. One end of the specimens was assumed to be fixed, and the other end was free. The initial velocity of the impactor was imposed by the command *INITIAL VELOCITY RIGID BODY.

Surface-to-surface contact elements were used to simulate the interface between the impactor and GFRP, the concrete and GFRP tube, and even the concrete and steel tube. This type of contact considers slip and separation. Hence, slip/debonding is displayed if either occurs between the concrete surface and GFRP surface, and between the concrete surface and steel surface (Abdelkarim and ElGawady 2014).

The friction coefficient was taken as 0.22 for the contact surface of the outer GFRP tube and concrete core, 0.25 for the contact surface of steel impactor and outer GFRP tube, as well as the inner steel tube and concrete, respectively (Jiang and Chorzepa 2014).

Comparison of numerical and experimental results

The damage modes of simulated specimens C7-III and D7-III are shown in Fig.10. For specimen C7-III, the maximum longitudinal compressive stress occurred at the loading point, and the maximum longitudinal tensile stress occurred at the fixed end, resulting in resin crushing at the loading point and fiber rupture in the hoop direction at the fixed end. The maximum lateral tensile stress of C7-III occurred on both sides of the loading point, while the lateral compressive stress was much lower than the longitudinal compressive stress. For specimen D7-III, the maximum longitudinal tensile stress occurred simultaneously at the loading area and the fixed end, resulting in local buckling and crushing at the loading area. The distribution of lateral stress of D7-III was similar with that of C7-III.

The numerical and experimental impact load-time histories of CFFT and concrete filled FRP-steel DSTC specimens were shown in Fig.11. The numerical curves in Fig.11 showed that the model offered reasonable trend with the test data, i.e., FE analyses is capable of capturing the overall shapes of the tested impact load-time histories. Table 3 reveals that the numerical peak impact loads are in good agreement with the experimental values.

Influence of axial loads

For composite columns used as bridge piers, they are designed to carry the vertical load from superstructures. Due to the limit of impact test system, our test specimens were not applied with the axial loads. Thus, the verified FE models were used to investigate the influence of axial loads on the impact responses of composite columns. The axial compression ratio (ACR) of CFFTs is defined as

$$\lambda = \frac{N}{f_F A_F + f_C A_C} \tag{2}$$

where N is the axial load applied on the columns, f_F and A_F are the axial compression strength and cross-sectional area of FRP tubes, respectively, and f_c and A_c are the confined strength of concrete and cross-sectional area of FRP tubes, respectively. The confined strength of concrete in CFFTs can be obtained from Lam and Teng (2003). The axial compression ratio of concrete filled FRP-steel DSTCs is defined as

$$\lambda' = \frac{N}{f_F A_F + f_c' A_c + f_s A_s} \tag{3}$$

where f_s and A_s are the confined strength of concrete and cross-sectional area of FRP tubes, respectively. The confined strength of concrete in concrete filled FRP-steel DSTCs can be obtained from Teng et al. (2002).

According to GB 50010 (GB 2010), the maximum value of ACR of concrete columns is less than 0.65. The impact load histories of C7-II and D7-II with ACRs 0, 0.2 and 0.6 were calculated, respectively. It is shown in Fig.12 that the ACR has insignificant influence on the impact load history of C7-II. However, the peak impact load of D7-II decreases by 33% when the ACRs increase from 0 to 0.6. This is because global buckling is more prone to occur in concrete filled FRP-steel DSTCs under compression compared with CFFTs.

Influence of impact height

Three different impact heights (i.e., 0.5, 1.0, and 1.5 m) are tried on C7-II and D7-II specimens, respectively. Each specimen is impacted only once. Fig 13 shows the impact load histories of C7-II and D7-II specimens under different impact heights. When the impact height is less than 1.0 m, it has insignificant influence on the impact load histories of C7-II. Further increasing the impact height from 1.0 m to 1.5 m resulted in 27% decrease of peak impact load of C7-II. On the other hand, the increases of impact height from 0.5 m to 1.5 m result in gradually decrease of peak impact load of D7-II.

Analytical model of the impact responses

In the derivation of the deformation responses of a composite column under lateral impact, a test specimen was assumed to be axially inextensible and follow the Euler–Bernoulli beam theory where shear deformation and rotary inertia terms are neglected. The boundary conditions are considered to be clamp-free.

Material models

The differential equation for lateral displacement of a uniform cantilever beam subjected to impact is shown as (Brillouin 1960; Alper and Daniel 2011)

$$m\frac{\partial^{2}W(x,t)}{\partial t^{2}} + C\frac{\partial W(x,t)}{\partial t} + EI\frac{\partial^{4}W(x,t)}{\partial x^{4}} = P(x,t)$$
(4)

where W(x, t) is the lateral displacement, m = mass of the beam per unit length, C = damping intensity of the beam, E = Young's modulus of the materials, I = inertia of the cross section and P(x, t) = impact function.

W(x, t) can be considered as the sum of a series of products of spatial functions of only x and time-dependent functions as

$$W(x,t) = \sum_{i=1}^{\infty} \phi_i(x) w_i(t)$$
 (5)

where $\phi_i(x)$ are the eigenfunctions of a linear uniform cantilever beam and $w_i(t)$ are the generalized time-dependent coordinates.

Substituting Eq. (5) into Eq. (4), multiplying $\phi_j(x)$ on both sides of Eq. (4) and then integrating each term of Eq. (4) over span l, we obtained (Wang et al. 2017)

$$\int_{0}^{\infty} \frac{P(x,t)\phi_{i}(x)}{m} dx \tag{6}$$

in which

$$\xi_i = \frac{c}{2m\omega_i}$$

where ω_i is the eigenvalue of a linear uniform cantilever beam.

The expression of impact force P(x, t) is assumed as a dual function, as shown in Fig.14. In the first phase, the impact load increased linearly with time. In the second phase, the impact load decreased with time, which was simulated by an exponential function. Thus, the impact function can be expressed as follows:

$$P(x,t) = \begin{cases} \frac{P_0}{t_1} t \delta(x - l_0) & 0 \le t \le t_1 \\ P_0 \cdot e^{-a(t - t_1)} \delta(x - l_0) & t_1 < t \end{cases}$$
(7)

where P_0 and t_1 are the peak impact load and the corresponding time, respectively. δ is the unit pulse function, l_0 is the distance between the loading point and the clamped end of the beam, and a is a factor which is determined by fitting the decrease phase with the exponential function.

The vibration equation of modal coordinates can be obtained by substituting Eq. (7) into Eq.(6).

In the case of $0 \le t \le t_1$,

$$v_{i1}(t) = \frac{k_i P_0}{t_1} t$$
 (8)

where,
$$k_i = \frac{\phi_i(l_0)}{m \int_0^l \phi_i^2(x) dx}$$

The solution of w_{i1} is

$$w_{i1}(t) = \frac{k_i P_0}{t_1 \omega_i^3} \left[2\xi_i \cos(\omega_i \sqrt{1 - \xi_i^2} t) + \frac{2\xi_i^2 - 1}{\sqrt{1 - \xi_i^2}} \sin(\omega_i \sqrt{1 - \xi_i^2} t) \right] e^{-\xi_i \omega_i t} - \frac{2\xi_i k_i p_0}{t_1 \omega_i^3} + \frac{k_i p_0}{t_1 \omega_i^2} t$$
(9)

In the case of $t_1 < t$,

$$v_{i2}(t) = k_i P_0 \cdot e^{-a(t-t_1)}$$
(10)

The solution of w_{i2} is

$$w_{i2}(t) = \left[A_i \cos(\omega_i \sqrt{1 - \xi_i^2} t) + B_i \sin(\omega_i \sqrt{1 - \xi_i^2} t) \right] e^{-\xi_i \omega_i t} + \frac{k_i P_0}{(a^2 - 2a\xi_i \omega_i + \omega_i^2)} e^{-a(t - t_1)}$$
(11)

When $t=t_1$, $w_{i1}(t_1)=w_{i2}(t_1)$, v_1, v_2, v_3 . Thus v_i and v_i for a cantilever beam were obtained as follow

$$A_{i} = \frac{2\xi_{i}k_{i}P_{0}}{t_{1}\omega_{i}^{3}} - k_{i}P_{0}e^{\xi_{i}\omega_{i}t_{1}} \left(\frac{2\xi_{i}}{t_{1}\omega_{i}^{3}} - \frac{1}{\omega_{i}^{2}} + \frac{1}{a^{2} - 2a\xi_{i}\omega_{i} + \omega_{i}^{2}}\right) \cos(\omega_{i}\sqrt{1 - \xi_{i}^{2}}t_{1})$$

$$+ \frac{k_{i}P_{0}}{\omega_{i}\sqrt{1 - \xi_{i}^{2}}}e^{\xi_{i}\omega_{i}t_{1}} \left(\frac{2\xi_{i}^{2} - 1}{t_{1}\omega_{i}^{2}} + \frac{\xi_{i}\omega_{i} - a}{a^{2} - 2a\xi_{i}\omega_{i} + \omega_{i}^{2}} - \frac{\xi_{i}}{\omega_{i}}\right) \sin(\omega_{i}\sqrt{1 - \xi_{i}^{2}}t_{1})$$

$$B_{i} = \frac{k_{i}P_{0}\left(2\xi_{i}^{2} - 1\right)}{t_{1}\omega_{i}^{3}\sqrt{1 - \xi_{i}^{2}}}$$

$$-k_{i}P_{0}e^{\xi_{i}\omega_{i}t_{1}} \left(\frac{2\xi_{i}}{t_{1}\omega_{i}^{3}} - \frac{1}{\omega_{i}^{2}} + \frac{1}{a^{2} - 2a\xi_{i}\omega_{i} + \omega_{i}^{2}}\right) \sin(\omega_{i}\sqrt{1 - \xi_{i}^{2}}t_{1})$$

$$+ \frac{k_{i}P_{0}}{\omega_{i}\sqrt{1 - \xi_{i}^{2}}}e^{\xi_{i}\omega_{i}t_{1}} \left(\frac{1 - 2\xi_{i}^{2}}{t_{1}\omega_{i}^{2}} + \frac{a - \xi_{i}\omega_{i}}{a^{2} - 2a\xi_{i}\omega_{i} + \omega_{i}^{2}} + \frac{\xi_{i}}{\omega_{i}}\right) \cos(\omega_{i}\sqrt{1 - \xi_{i}^{2}}t_{1})$$

$$(13)$$

Substituting Eqs. (12) and (13) into Eq. (11), and then substituting Eqs. (9) and (11) into Eq. (5), the displacement responses of a cantilever beam subjected to lateral impact can be obtained.

Comparison of analytical and experimental results

The damping ratios of the test specimens were obtained from the logarithmic decrement of displacement histories (Fig. 7). The first three modes were used for the calculation. It is assumed that no delamination between concrete core and outer/inner tubes occurred under impact. The effective bending stiffness of CFFTs (*EI*)_{eff} presented in Wang et al. (2017) was used to predict the displacement responses of test specimens subjected to lateral impact, as given by

$$(EI)_{eff} = \frac{E_f \pi}{4} \left\{ \alpha \left[\left(r + t_1 \right)^4 - r^4 \right] + \beta r^4 n^2 \right\}$$
(14)

where E_f is Young's modulus of outer FRP tubes, r and t_1 are the inner radius and wall thickness of FRP tubes, and α =0.15 and β =0.5 are the reduction factors of FRP and concrete due to impact damage (Wang et al. 2017), respectively.

Considering the effect of impact damage of FRP and concrete on the bending stiffness of hybrid columns, the concrete area is converted into equivalent the FRP area by applying the modular ratio n, and then the effective bending stiffness of concrete

filled FRP-steel DSTCs $(EI)'_{eff}$ is given as

$$(EI)_{eff}' = E_s I_s + \frac{E_f \pi}{4} \left\{ \alpha \left[\left(r_1 + t_1 + t_2 \right)^4 - \left(r_1 + t_1 \right)^4 \right] + \frac{n^2 \beta \left[\left(r_1 + t_1 \right)^2 - r_1^2 \right]^2}{4} \right\}$$
(15)

where E_s and I_s are the Young's modulus and inertia of steel tubes, r_1 and t_2 are the outer radius of steel tubes and wall thickness of concrete, respectively.

The reduction factors of FRP and concrete in the concrete filled FRP-steel DSTCs are deemed as the same as those of in CFFTs. The bending stiffness of steel tubes were not discounted because the no local buckling occurred in the inner steel tubes of concrete filled FRP-steel DSTCs under impact.

Eqs. (14) and (15) were used to calculate the effective bending stiffness of CFFTs and concrete filled FRP-steel DSTCs. Comparisons of the analytical and the measured maximum displacements at the loading point showed good agreement, as given in table 4.

Conclusions

A series of horizontal impact tests were conducted to investigate the responses of CFFT and concrete filled FRP-steel DSTC specimens, in which the influences of impact velocity and thickness of GFRP tubes were considered. The impact process, time histories of impact load, acceleration, displacement and impact energy of the specimens were instrumented and analyzed. The results obtained from this study are summarized as follows:

- (1) Circular cracks at the fixed end and crushing of GFRP at the loading point are prevalent in the CFFTs and concrete filled FRP-steel DSTCs. Under the same applied impact energy, the concrete filled FRP-steel DSTCs have more severe damages at the loading point and smaller damage area at the fixed end than CFFTs. Moreover, the maximum and residual lateral deformations of concrete filled FRP-steel DSTCs were much lower than those of CFFTs. It indicated that concrete filled FRP-steel DSTCs have lower local stiffness and higher global stiffness than CFFTs.
- (2) Higher impact velocity resulted in higher maximum displacement, higher peak impact load and heavier damage, thus resulting in higher residual deformations. Thicker GFRP tubes resulted in a little increment of peak impact load and a little reduction of duration of both CFFT and concrete filled FRP-steel DSTCs. Moreover, increasing the GFRP thickness from 7 mm to 10 mm has insignificant effect on maximum displacement and energy absorption of CFFT and concrete filled FRP-steel DSTC specimens. Under the same impact velocity, the concrete filled FRP-steel DSTCs absorbed more energy than CFFTs.
- (3) The dynamic analysis program (LS-DYNA) provided reasonable simulation of the experimental results of the impact load-time histories for both hollow and concrete filled GFRP tubes. Moreover, the FE model was used to investigate the influence of axial loads and impact height.

(4) The impact load histories were simulated by a dual function. The impact damage of GFRP tubes and concrete were considered in obtaining the effective bending stiffness. Then the Euler -Bernoulli model for lateral displacement of a cantilever beam under impact was used to predict the dynamic displacements, and analytical results agree well with test results.

Acknowledgments

The financial support from the National Natural Science Foundation of China (Grant No.51578283), Modern Science and Technology Support Program of Jiangsu Construction Industry of China (Grant No. 2016-13) and Top Six Talent Projects in Jiangsu Province, China (Grant No. JZ-024) are greatly appreciated. Partial funding of this research was provided by the U.S. National Science Foundation Grant IIP 1230351.

Reference

- Mirmiran, A. and Shahawy, M. (1996). "A new concrete-filled hollow FRP composite column". *Composites Part B*, 27B, 263-268.
- Fam, A., Pando, M., Filtz, G., and Rizkalla, S. (2003). "Precast composite piles for the route 40 bridge in Virginia using concrete-filled FRP tubes". *PCI Journal*, 48(3), 32–45.
- GangaRao, H., Taly, N., and Vijay, P.V. (2007). "Reinforced concrete design with FRP composites". USA: Taylor & Francis Group.
- Teng, J.G., Yu, T., Wong, Y.L., and Dong, S.L. (2007). "Hybrid FRP-concrete-steel tubular columns: Concept and behavior". *Construct. Build. Mater.*, 21, 846-854.
- Lam, L. and Teng, J.G. (2003). "Design-oriented stress-strain model for FRP-confined concrete". *Construct. Build. Mater.*, 17, 471-489.
- Xie, P., Yu, T., Wong, Y.L., and Teng, J.G. (2011). "Compressive behavior of large scale hybrid FRP concrete steel double skin tubular columns". *Advanced Materials Research*, 243–249, 1138–1144.
- Dagher, H., Bannon, D.J., Davids, W.G., Lopez-Anido, R.A., and Nagy, E. (2012). "Bending behavior of concrete-filled tubular FRP arches for bridge structures". *Construct. Build. Mater.*, 37, 432-439.
- Yu, T., Wong, Y.L., Teng, J.G., Dong, S.L., and Lam, E.S.S. (2006). "Flexural behavior of hybrid FRP-concrete-steel double-skin tubular members". *J. Compos. Constr.*, 10(5), 443–452.
- Li, B., Zohrevand, P., and Mirmiran, A. (2013). "Cyclic behavior of FRP concrete bridge pier frames". *Journal of Bridge Engineering*, 18(5), 429-438.
- Pham, T.M. and Hao, H. (2017). "Axial impact resistance of FRP-confined concrete". *J.Compos. Constr.*, 21(2): 04016088
- Huang, L., Sun, X., Yan, L., and Kasal, B. (2017). "Impact behavior of concrete columns confined by both GFRP tube and steel spiral reinforcement". *Construct. Build. Mater.*, 131: 438-448.

- Huang, L., Gao, C., Yan L., Yu, T., and Kasal B. (2018). "Experimental and numerical studies of CFRP tube and steel spiral dual-confined concrete composite columns under axial impact loading". *Composites Part B*, 152, 193-208
- Xiao, Y., and Shen, Y. (2012). "Impact behaviors of CFT and CFRP confined CFT stub columns". *J. Compos. Constr.*, 16(6), 662–670.
- Alam, M. I., F, S., and Liu, X. (2015). "Effect of bond length on the behaviour of CFRP strengthened concrete-filled steel tubes under transverse impact". *Composite Structures*, 132, 898-914.
- Qasrawi, Y., Heffernan, P.J., and Fam, A. (2015). "Dynamic behaviour of concrete filled FRP tubes subjected to impact loading". *Engineering Structures*, 100, 212-225.
- Chen, C., Zhao, Y., and Li, J. (2015). "Experimental investigation on the impact performance of concrete-filled FRP steel tubes". *J. Eng. Mech.*, 141(2), 04014112.
- Abdelkarim, O.I. and ElGawady, M.A. (2016). "Performance of hollow-core FRP-concrete-steel bridge columns subjected to vehicle collision". Engineering Structures, 123, 517-531.
- Wang, R., Han, L., and Tao, Z. (2015). "Behavior of FRP-concrete-steel double skin tubular members under lateral impact: experimental study." Thin-Walled Structures, 95, 363-373.
- Wang, J., GangaRao, H., Liang, R., and Liu, W. (2017). "Experimental and analytical responses of hollow and concrete-filled GFRP tube columns under impact". *J. Compos. Constr.*, 04017013.
- Liu, Q., Zhou, D., Wang, J., and Liu, W. (2018). "Mechanical behavior of FRP confined steel tubular columns under impact". *Steel and Composite Structures*, 27(6): 691-702.
- Metallic materials-Tensile testing-Part 1: Method of test at room temperature. GB/T 228.1-2010, ISO 6892-1:2009, MOD.
- Singh, N.K. and Singh, K.K (2014). "Review on impact analysis of FRP composites validated by LS-DYNA". *Polymer Composites*, DOI: 10.1002/pc.23064
- Standard test method for compressive strength of cylindrical concrete specimens. ASTMC39/C39M 12.
- Murray, Y.D. (2007). "Users manual for LS-DYNA concrete material model 159". *Report No. FHWAHRT-05-062*, Federal Highway Administration.
- Adhikary, S.D., Li,B., and Fujikake, K. (2015). "Low velocity impact response of reinforced concrete beams: experimental and numerical investigation". *Int. J. Prot. Struct.*, 6(1), 81-111.
- Guo, W., Fan, W., Shao, X., Shen, D., and Chen, B. (2018). "Constitutive model of ultra-high-performance fiber-reinforced concrete for low-velocity impact simulations", *Composite Structures*, 185, 307-326.
- Hu, C., Han, L., and Huo, C. (2018). "Concrete-encased CFST members with circular sections under laterally low velocity impact: analytical behavior", *Journal of Constructional Steel Research*, 146,135-154.
- Brillouin, L. (1960). Wave propagation and group velocity, Academic Press, New

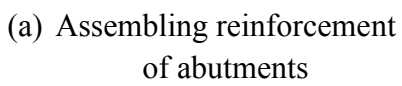
York.

- Liu, M. and Qian, J. (2007). "Moment-curvature relationships of FRP-concrete-steel double-skin tubular members". *J. Tsinghua Univ. (Sci. & Tech.*), 47(12): 2105-2110.
- Guades, E., Aravinthan, T., Manalo, A., Islam, M. (2013). "Damage modeling of repeatedly impacted square fibre-reinforced polymer composite tube". *Materials and Design*, 47, 687-697.
- Teng, J.G., Chen, J.F., Smith, S.T. and Lam, L. (2002). FRP: Strengthened RC structures, Wiley, UK.
- GB. (2010). "Code for design of concrete structure." *GB50010*, China Architecture & Building Press, Beijing, China.



Fig.1 Horizontal impact test system







(b) Concrete placement



(c) Finished specimens

Fig. 2 Fabrication of specimens

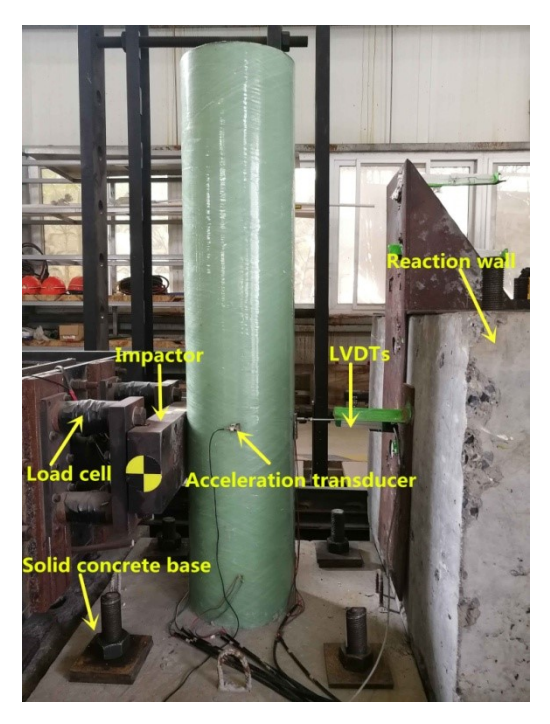


Fig.3 Test set- up

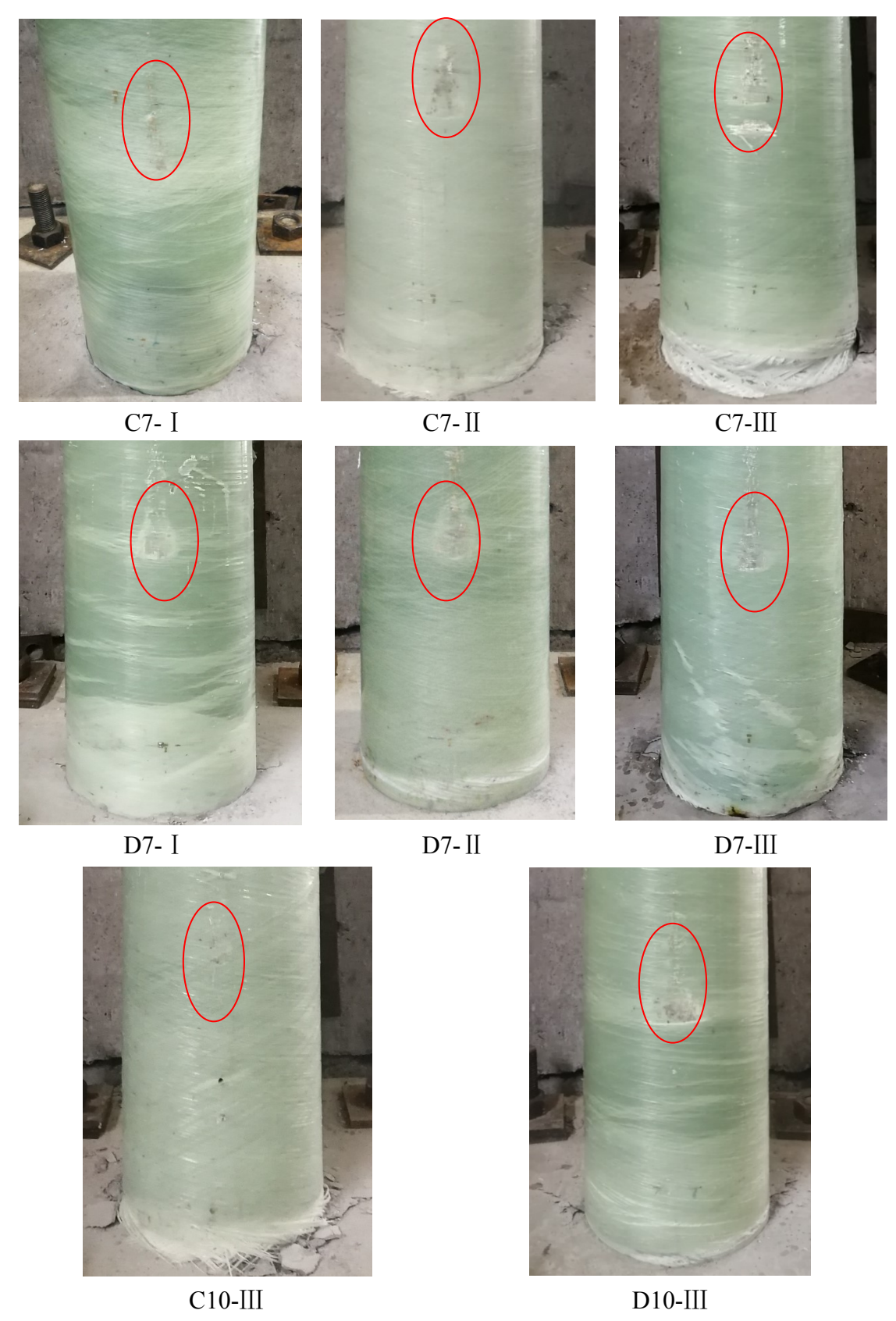


Fig.4 Impact damages

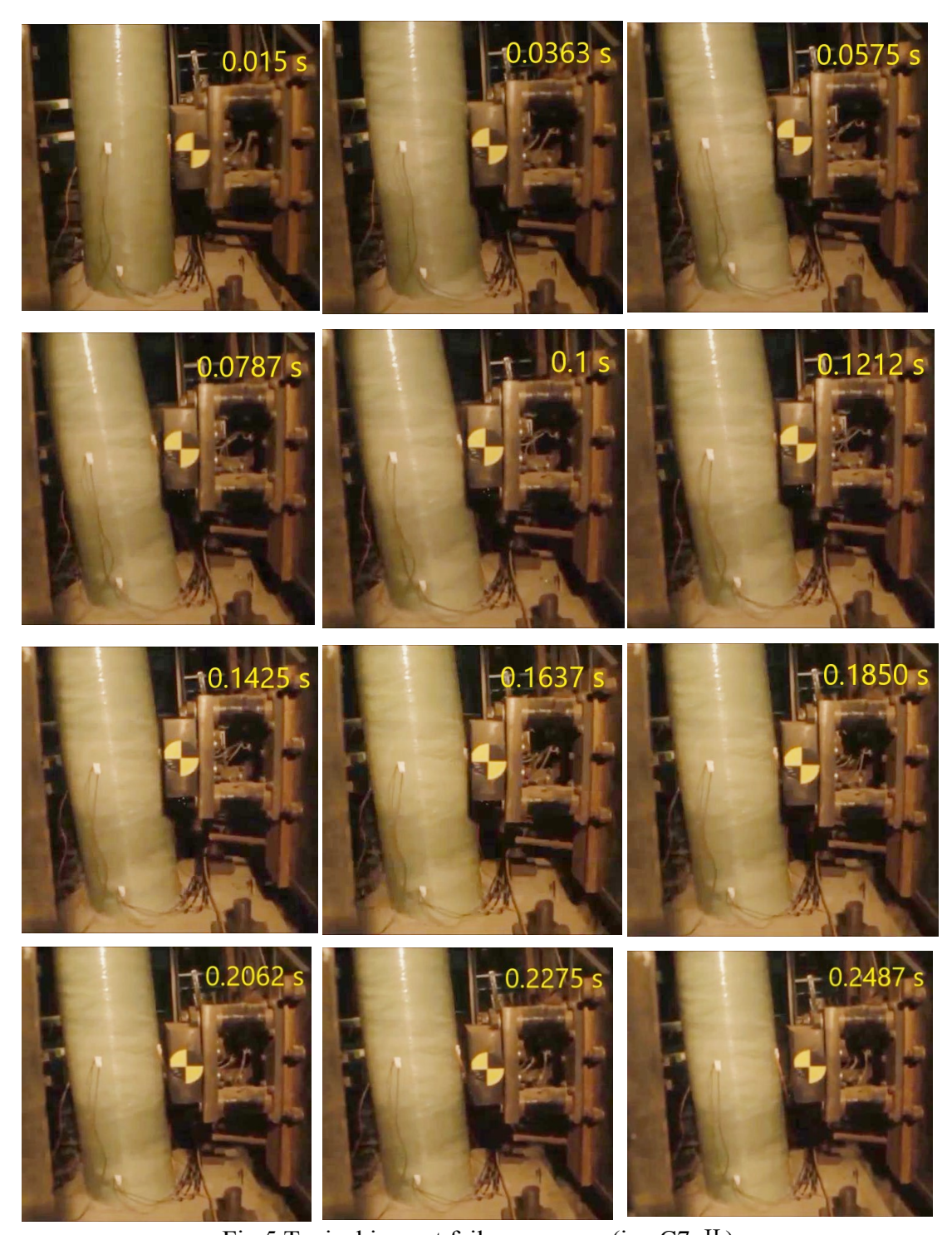


Fig.5 Typical impact failure process (i.e. C7-II)

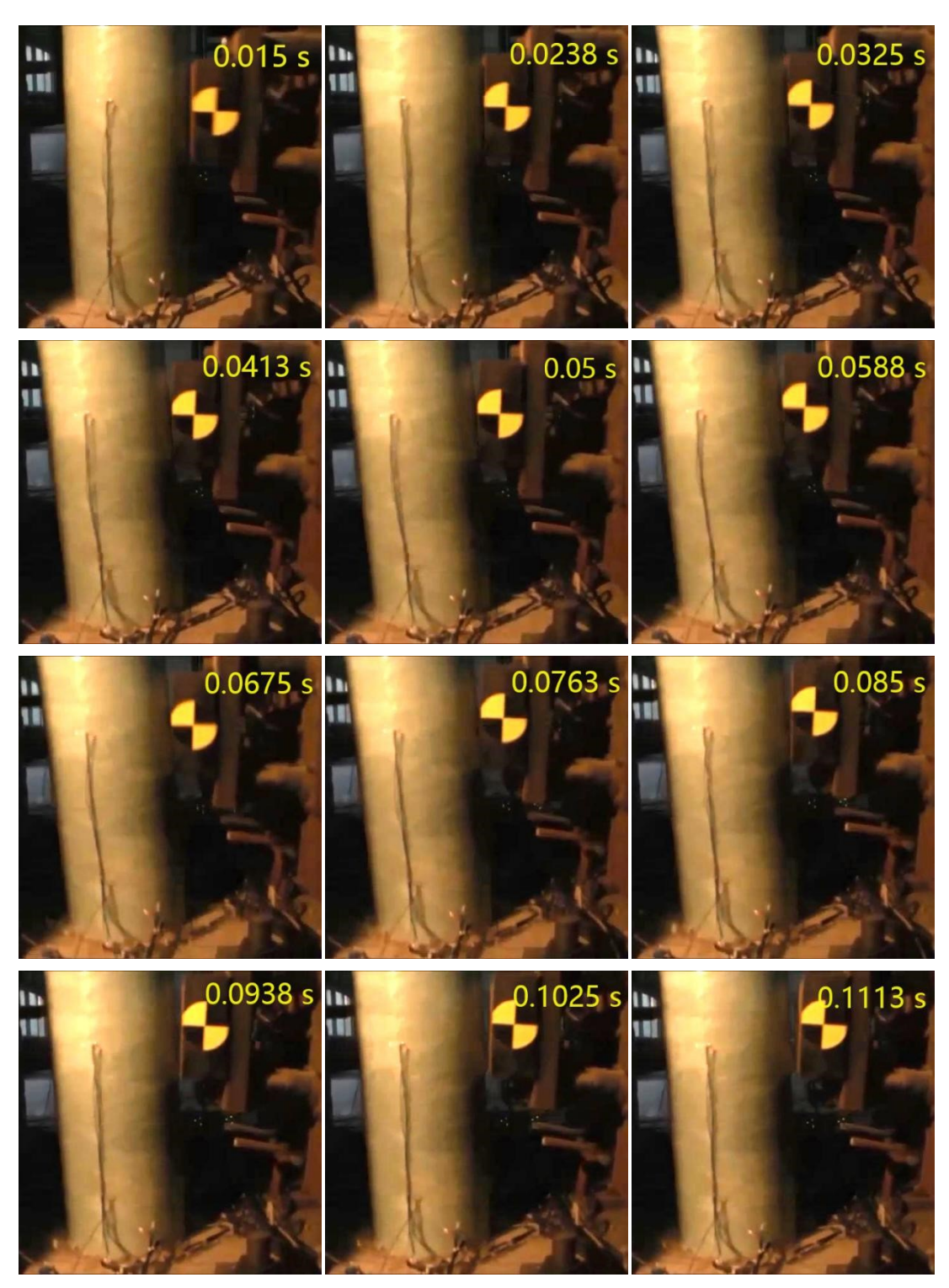


Fig.6 Typical impact failure process (i.e. D7-II)

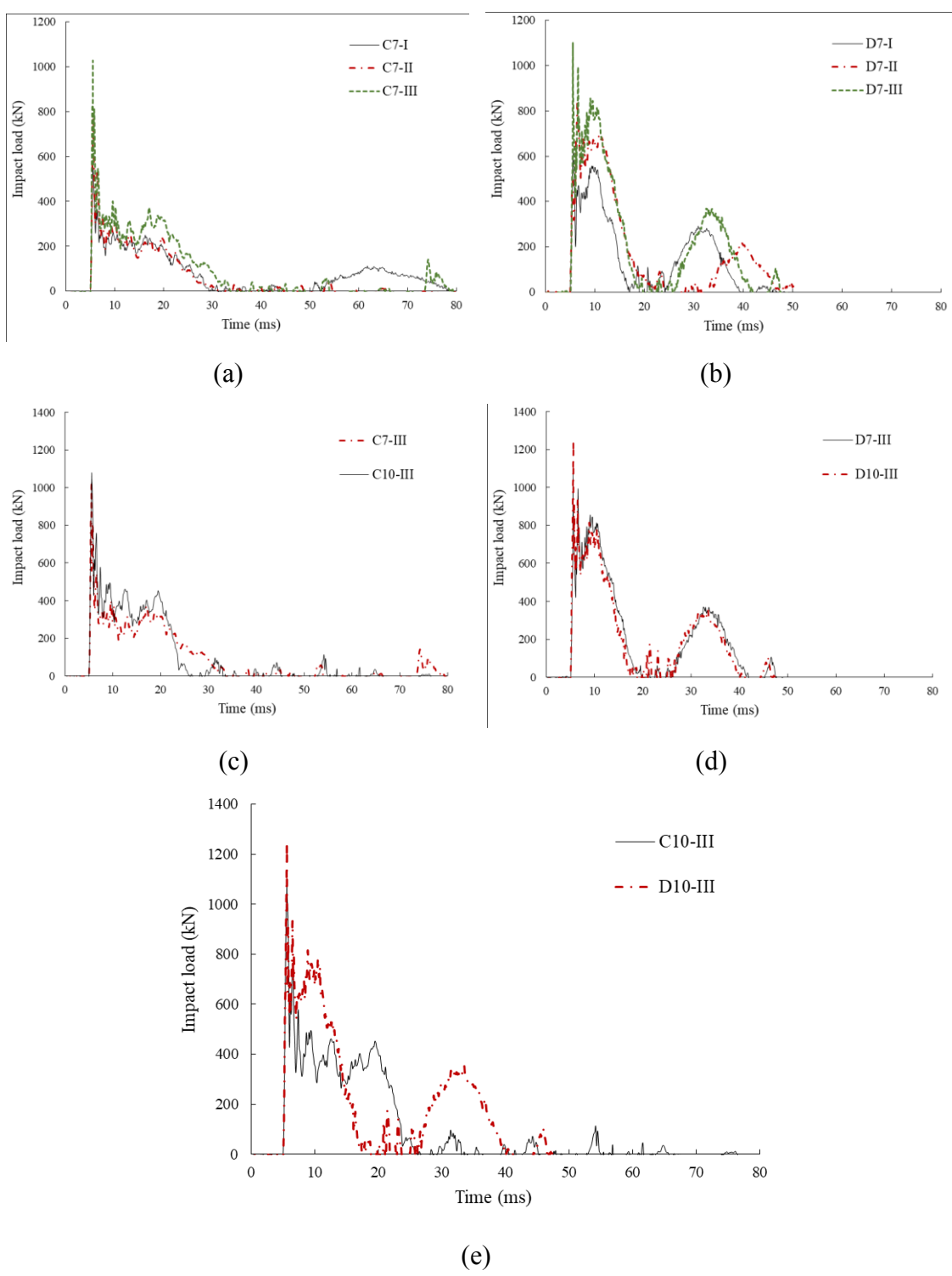


Fig.7 Impact load-time histories

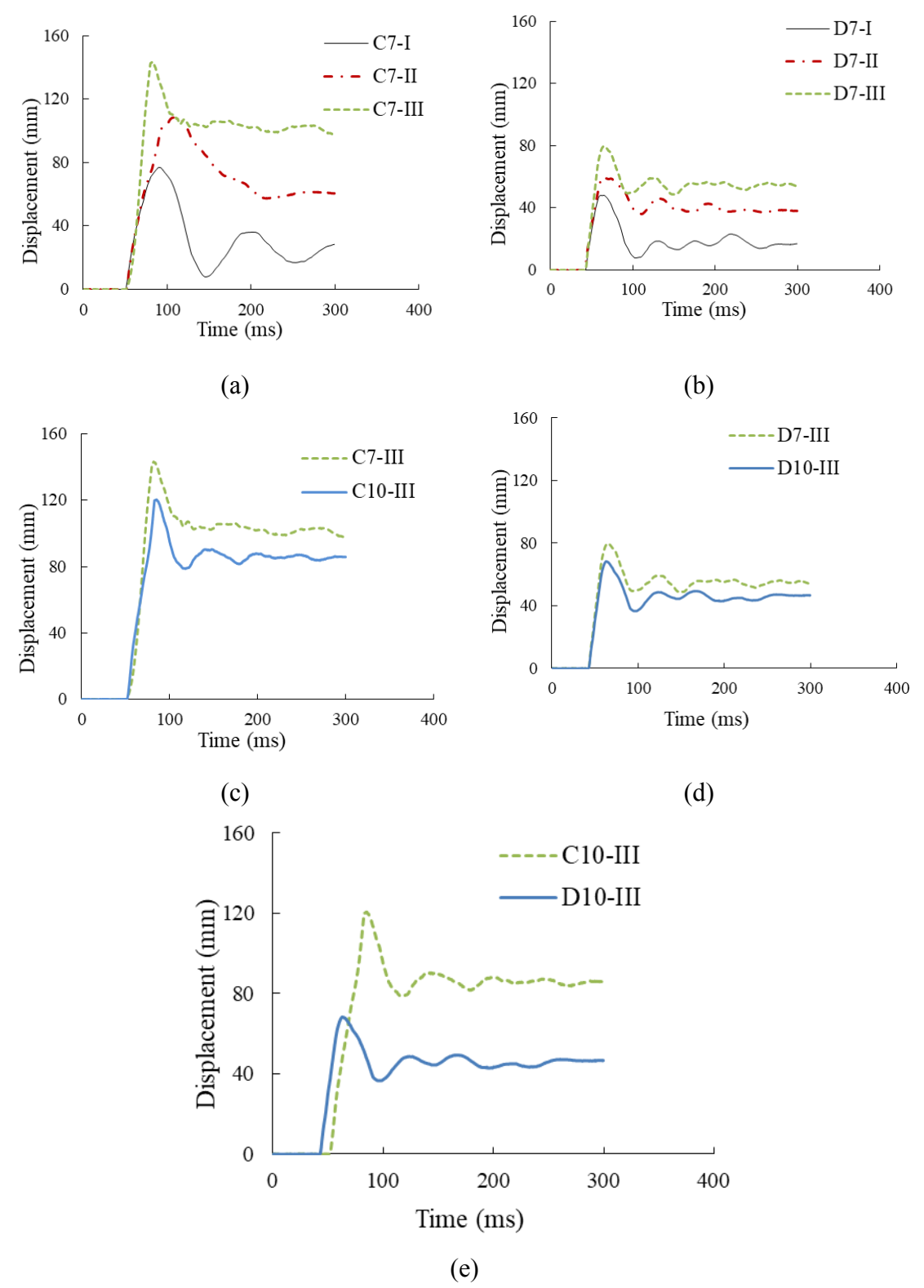


Fig.8 Displacement histories

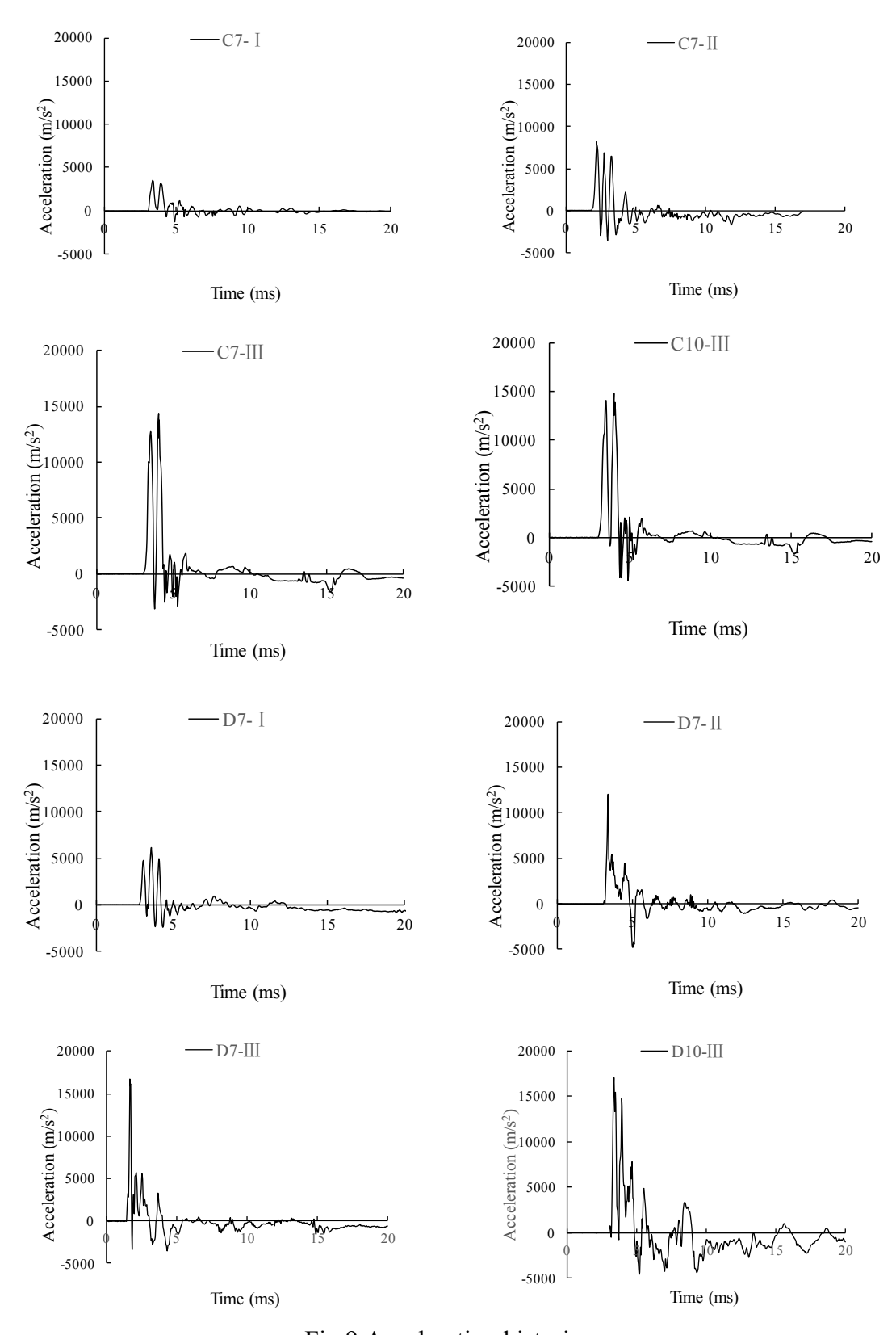


Fig.9 Acceleration histories

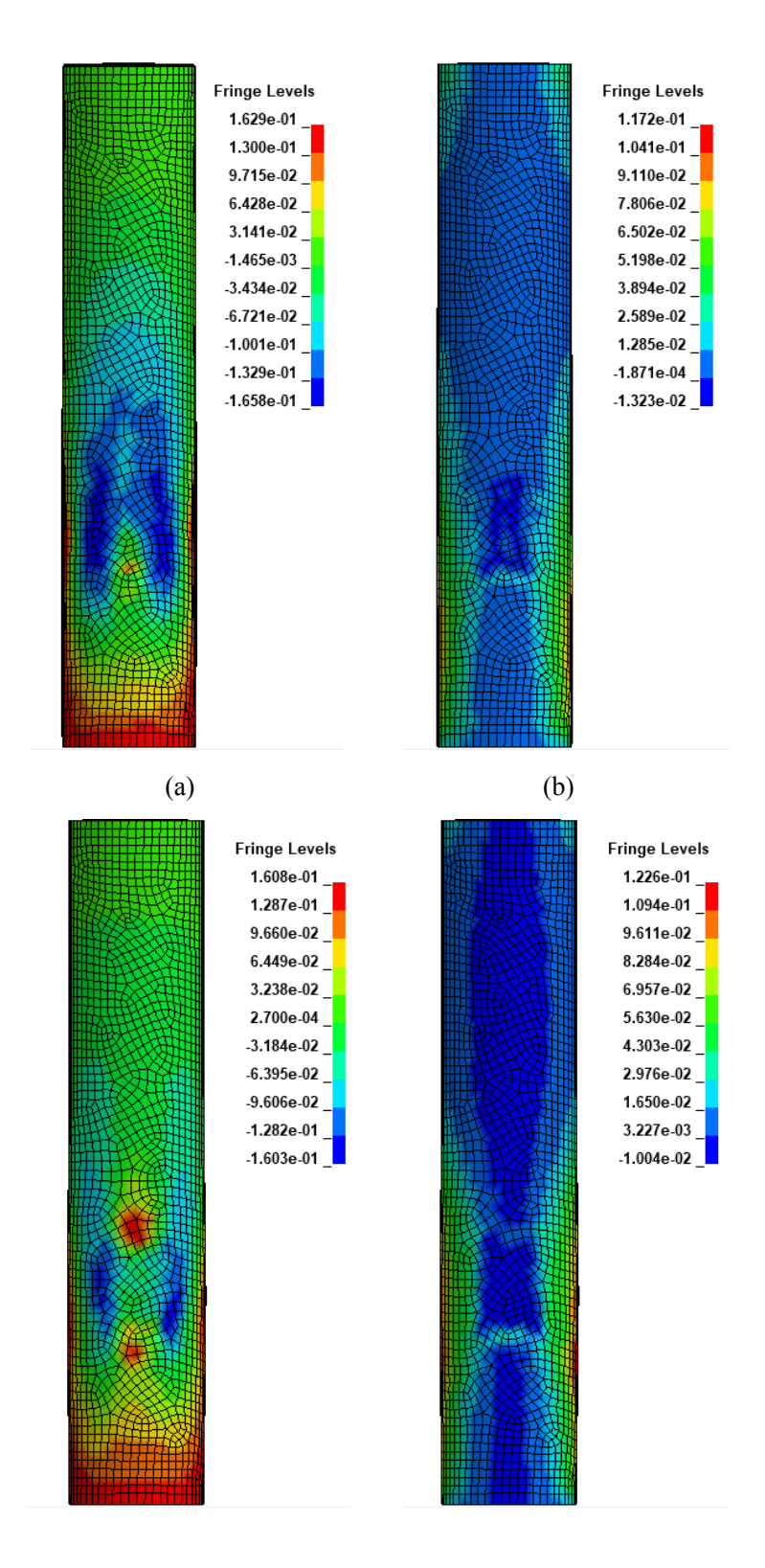


Fig. 10 Stress contour at failure (unit: GPa): (a) C7-III (longitudinal stress); (b) C7-III (lateral stress); (c) D7-III (longitudinal stress); (d) D7-III (lateral stress)

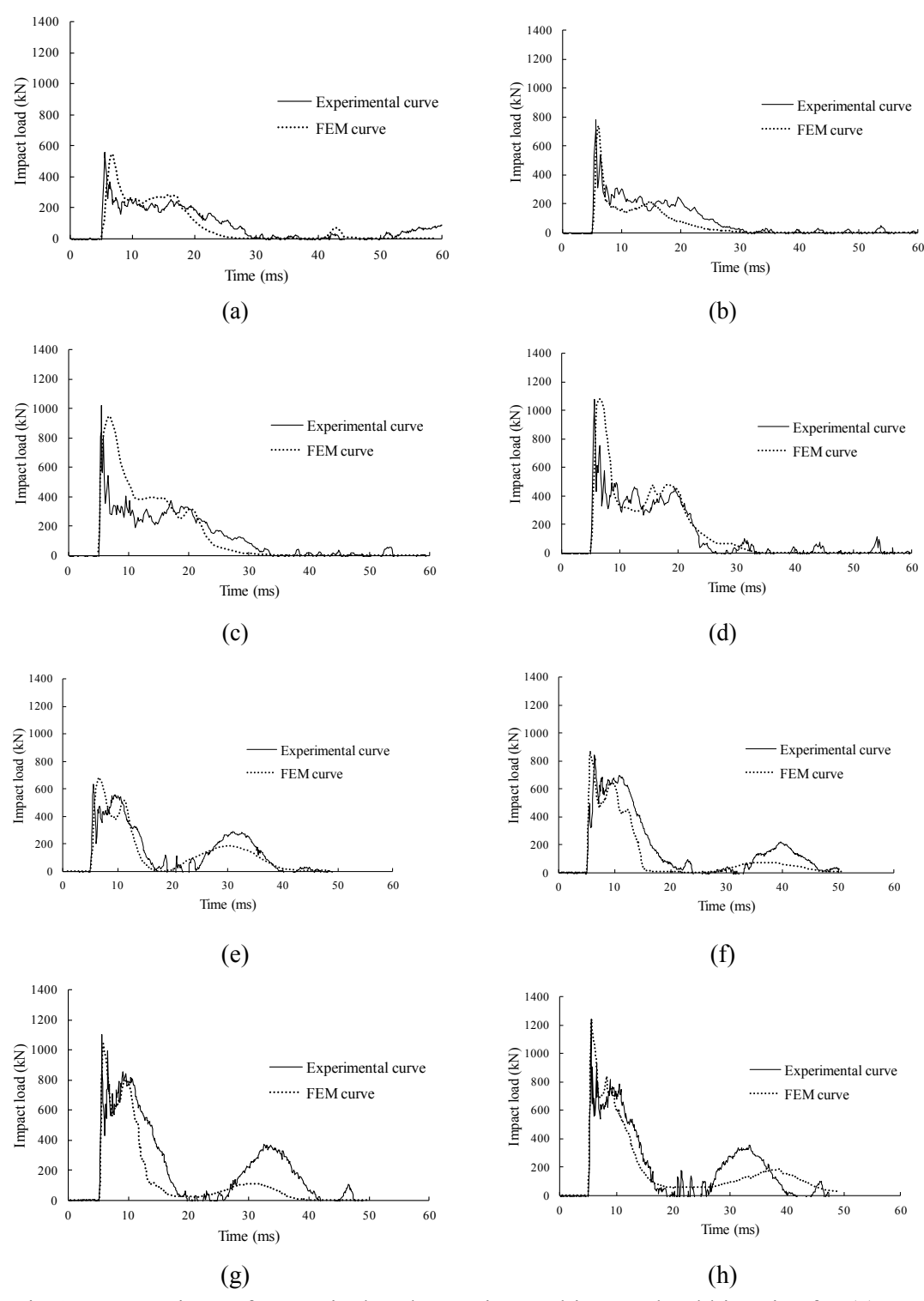


Fig.11 Comparison of numerical and experimental impact load histories for (a) C7-I; (b) C7-II; (c) C7-III; (d) C10-III; (e) D7-I; (f) D7-II; (g) D7-III and (h) D10-III

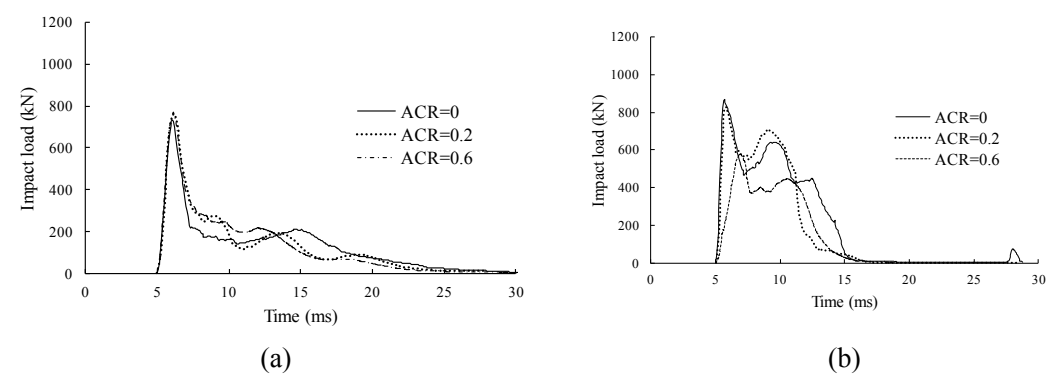


Fig.12 Simulated impact load histories of specimens with different axial compression ratios for (a) C7-II and (b) D7-II

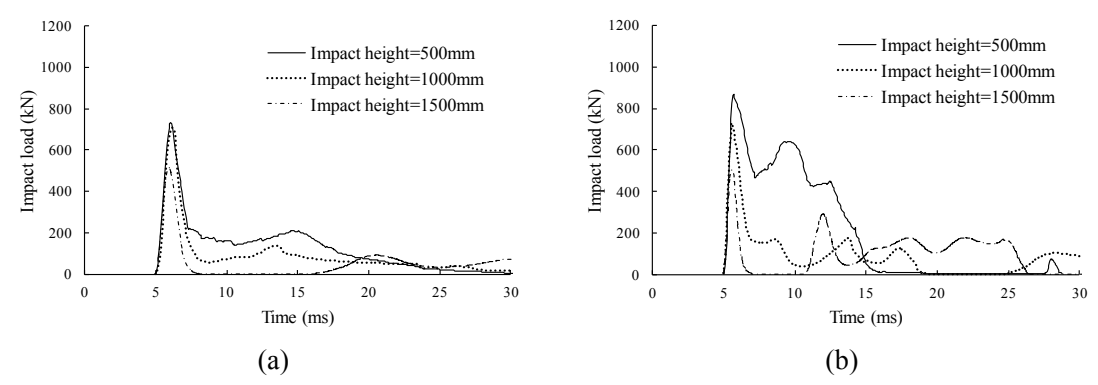


Fig.13 Simulated impact load histories of specimens with different impact heights for (a) C7-II and (b) D7-II

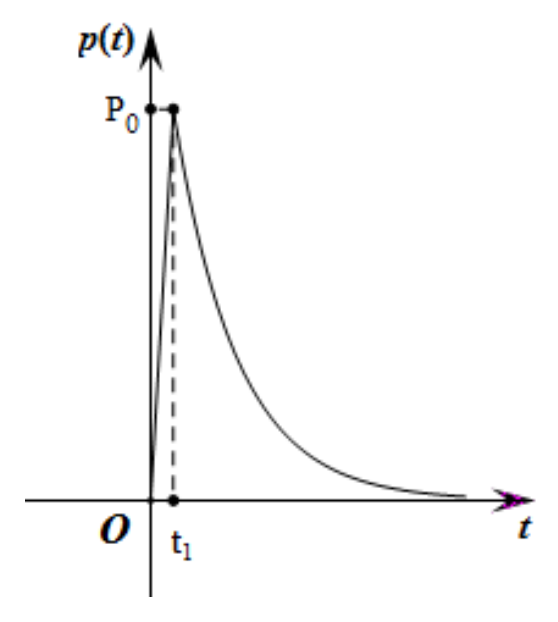


Fig.14 Sketch of a dual function to simulate the impact load histories

Table 1 Test results

	Peak load	D .:	Maximum	Residual	Maximum	Energy
Specimen	of impact	Duration (ms)	deformation	deformation	acceleration	absorption
	$P_{\rm i}({\rm kN})$		(mm)	(mm)	(m/s^2)	(J)
C7-I	554.3	24.4	77.0	27.0	3477	11135
C7-II	781.4	26.0	108.4	60.5	8243	19197
C7-III	1022.0	29.0	143.4	97.3	14388	28171
C10-III	1079.9	20.9	120.6	86.0	14788	30177
D7-I	630.2	11.9	48.2	17.0	6112	12565
D7-II	841.1	16.2	59.3	38.1	12040	23016
D7-III	1101.8	16.1	79.8	54.0	16698	32113
D10-III	1243.0	14.4	68.4	46.7	17076	34713

Note: In the first column, the first letters C and D mean CFFTs and concrete filled FRP-steel DSTCs, respectively, the numbers 7 and 10 mean the thicknesses of GFRP tubes are 7 and 10 mm, respectively, and the last numbers $\, I$, $\, II$ and $\, III$ mean the applied impact velocities are 4.0 m/s, 5.5 m/s and 7.0 m/s, respectively.

Table 2 Mechanical properties of concrete

Density (kg/m³)	Compressive strength (MPa)	Young's modulus (GPa)	Poission's ratio	Failure strain	Maximum aggregate size (mm)	Initial damage
2500	22.5	28	0.2	0.2	20	0

Table 3 Comparison of peak impact loads between numerical and experimental results

Specimen	Tested peak impact load $P_1(kN)$	Numerical peak impact load P ₂ (kN)	$\delta = \frac{P_2 - P_1}{P_1} \times 100\%$
C7-I	554.3	547.9	-1.6
C7-II	781.4	734.9	-6.0
C7-III	1022.0	946.1	-7.4
C10-III	1079.9	1077.8	-0.2
D7-I	630.2	676.8	7.4
D7-II	841.1	867.4	3.1
D7-III	1101.8	1044.2	-5.2
D10-III	1243.0	1237.6	-0.4

Table 4 Comparison of maximum displacements between analytical and experimental results

	-		
	Tested maximum	Analytical maximum	$w_{-}-w_{-}$
Specimen	displacement	displacement	$\delta = \frac{w_2 - w_1}{w} \times 100\%$
	$w_1(mm)$	w_2 (mm)	w_1
C7-I	77.0	72.1	-6.4
C7-II	108.4	102.2	-5.7
C7-III	143.4	130.6	-8.9
C10-III	120.6	109.3	-9.4
D7-I	48.2	43.0	-10.8
D7-II	59.3	54.7	-7.8
D7-III	79.8	73.4	-8.0
D10-III	68.4	72.2	5.6